Charge, Color, and Conformation: Spectroscopy on Isomer-Selected Peptide Ions

Chang Min Choi, Anne-Laure Simon, Fabien Chirot, Alexander Kulesza, Geoffrey Knight, Steven Daly, Luke Macaleese, Rodolphe Antoine, Philippe Dugourd

▶ **To cite this version:**

Chang Min Choi, Anne-Laure Simon, Fabien Chirot, Alexander Kulesza, Geoffrey Knight, et al.. Charge, Color, and Conformation: Spectroscopy on Isomer-Selected Peptide Ions. Journal of Physical Chemistry B, 2016, 120 (4), pp.709-714. 10.1021/acs.jpcb.5b11919 . hal-01345016

HAL Id: hal-01345016
https://hal.science/hal-01345016

Submitted on 20 Jul 2016

HAL is a multi-disciplinary open access archive for the deposit and dissemination of scientific research documents, whether they are published or not. The documents may come from teaching and research institutions in France or abroad, or from public or private research centers.

L'archive ouverte pluridisciplinaire **HAL**, est destinée au dépôt et à la diffusion de documents scientifiques de niveau recherche, publiés ou non, émanant des établissements d'enseignement et de recherche français ou étrangers, des laboratoires publics ou privés.

Charge, Color and Conformation: Spectroscopy on Isomer Selected Peptide Ions

Chang Min Choi,[1] Anne-Laure Simon,[1] Fabien Chirot,[2] Alexander Kulesza,[1] Geoffrey Knight,[1] Steven Daly,[1] Luke MacAleese,[1] Rodolphe Antoine,[1] Philippe Dugourd[1,*]

[1]*Institut Lumière Matière, Université Lyon 1 – CNRS, Université de Lyon, 69622 Villeurbanne Cedex, France*

[2]*Institut des Sciences Analytiques, Université Lyon 1 – CNRS, Université de Lyon, 69622 Villeurbanne Cedex, France*

*** Correspondance to:** Philippe Dugourd, Email : phillipe.dugourd@univ-lyon1.fr

Abstract :

Monitoring the chromism induced by intramolecular hydrogen and charge transfers within proteins, as well as the isomerization of both protein and cofactor is not only essential to understand photo-active signaling pathways but also to design targeted opto-switchable proteins. We used a dual ion mobility drift tube coupled to a tunable picosecond laser to explore the optical and structural properties of a peptide chain bound to a chromophore – a prototype system allowing for a proton transfer coupled to conformational change. With the support of molecular dynamics and DFT calculations, we show how proton transfer between the peptide and its cofactor can dramatically modify the optical properties of the system and demonstrate that these changes can be triggered by collisional activation in the gas phase.

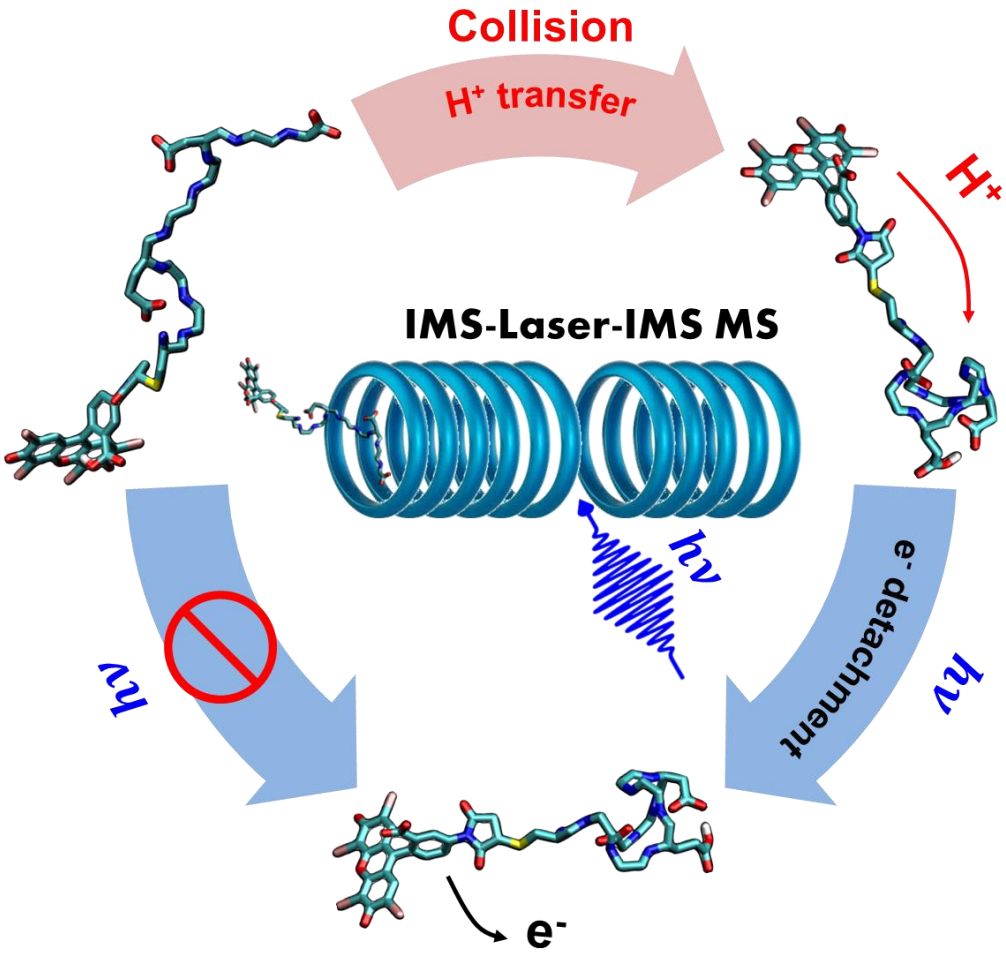

INTRODUCTION

Living cells constantly monitor their own state and their surroundings in order to respond effectively to changes in them. Photo-active signaling pathways rely on proteins with bound organic cofactors providing the possibility to sense light stimuli through cis-trans isomerization - such as in the vision process – or via electron and proton transfer reactions within and between proteins, which eventually trigger a series of biochemical reactions.[1–4] Both charge transfer and mechanical strain exerted by the protein environment can in turn dramatically change the optical properties of chromophores.[5,6] Thus, monitoring the chromism induced by intramolecular hydrogen and charge transfers, as well as the isomerization of the protein and cofactor is not only essential to understand life but also to design targeted photo-switchable proteins.[7–11] Gas phase experiments with the coupling of laser spectroscopy and ion mobility spectrometry (IMS)[12,13] have recently been used by Bieske and coworkers to provide information on the photoisomerization of charged photoactive molecules.[14,15] The present work parallels such studies in investigating the effects of collisionally activated isomerization. It opens a new way to probe opto-switching in proteins despite conformational heterogeneity among different individual copies of the same protein. Herein, we report first results on a prototype system allowing for a proton transfer coupled to conformational change: an acidic chromophore bound to a negatively charged host peptide. The chromophore is the fluorescein derivative Eosin Y (Eo) maleimide (see scheme in supporting information), which in solution has three absorption maxima which correspond to different protonation states.[16] The peptide sequence is CAAEAADAA, which was chosen to include several acidic residues to permit proton transfer between the chromophore and neighboring side chains of the host peptide. In the following Eo-P refers to the chromophore-peptide complex, where the chromophore is covalently bound to the thiol moiety of the cysteine residue. We used a dual ion mobility drift tube coupled to a tunable picosecond laser to measure the isomer-resolved optical spectroscopy of Eo-P anions to explore how the protonation state of the chromophore and the charged residues of the peptide influence the conformation and optical properties of the complex, and how collisional activation can be used to induce changes in those properties. The results are interpreted in light of molecular dynamics and DFT calculations.

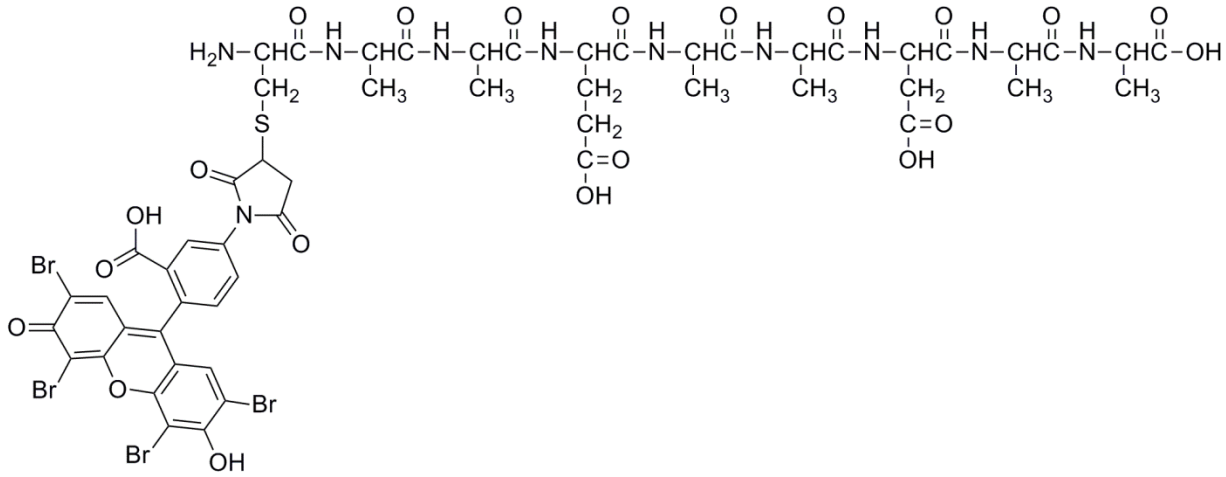

Scheme 1. Chemical structure for Eo-P. Deprotonation sites are the OH and COOH groups on eosin Y maleimide, the COOH groups at the side chain of Glu and Asp, and at the C terminus.

MATERIAL AND METHODS

Chemicals. The peptide H-CAAEAADAA-OH was purchased from GeneCust (Luxembourg) and was dissolved in H_2O to a concentration of 1.5mM. Eosin Y maleimide was dissolved in DMSO to a concentration of ~14mM. 15µL of this solution was added to 150 µL of the peptide solution. The resulting solution was left at room temperature for one hour to achieve EosinY maleimide tagging at the N terminus of the peptide. The solution was further diluted to a concentration of ~ 10µM and 0.1% of NH_4OH was added before electrospray.

Experiment. We used a tandem IMS instrument coupled to a high resolution time-of-flight mass spectrometer(Fig. 1).[17] It consists of two 79 cm long drift tubes (DT1 and DT2) connected by a dual ion funnel assembly (DF). The arrangement allows to select a particular isomer in a first IMS stage and then irradiate it with a tunable kHz picosecond optical parametric amplifier (PG400, EKPLA, Lithuania), the photo-products being separated in the second IMS stage before mass analysis. Activation by collisions is possible between the two IMS stages by applying an activation voltage between two electrodes in the middle of the dual ion funnel. In DT1 and DT2, Helium buffer gas is maintained at a pressure of ~4 Torr, the temperature T at 300 K and with typical voltage drops across DT1 and DT2 of 500 V. Experimental CCS are determined by measuring ion arrival times (AT) as a function of the inverse voltage value across DT2 and by fitting resulting values using Eq. 1.[18]

$$AT = t_0 + \frac{16}{3}\sqrt{\frac{\mu k_B T}{2\pi}}\frac{NL^2}{q\,CCS}\frac{1}{V} \qquad \text{Eq 1}$$

with μ the reduced mass for ion-buffer gas collisions, N the number density of the buffer gas, V the voltage across DT2 and L the drift length. t_0 corresponds to the transfer time of the ions from the end of DT2 to the detector.

Optical action spectra were obtained by irradiating selected ions in DF between DT1 and DT2 and monitoring the depletion of these ions as a function of the laser wavelength. The yield of depletion Y at each wavelength is given by:

$$\ln\left(\frac{I_0}{I}\right)/\varphi \propto Y \qquad \text{Eq. 2}$$

where φ is the laser fluence, I_0 and I the peak intensity without and with laser.
Reference spectra in Fig. 3a, 3d and 4 were recorded similarly but on *m/z* selected ions using a dual linear ion trap coupled to nanosecond optical parametric oscillator.[19]

Computational. We modelled the structure of Eosin-functionalized peptides in the gas phase by classical molecular dynamics based on the AMBER99 force field[20,21] within a generalized ensemble approach. We parametrized the Eosin chromophore in different charge and protonation states with the generalized Amber Force Field (GAFF)[22,23] and employed replica-exchange molecular dynamics[24] as implemented in Gromacs 5.0.2[25,26] to access low-energy conformations and generate canonical ensembles (see ref [27] for details). The lowest-energy structures were subsequently reoptimized at the DFT level using the hybrid functional CAM-B3LYP[28–30] for exchange and correlation, combined with Grimme's empirical dispersion correction including Becke-Johnson damping D3(BJ)[31,32]. DFT optimizations employ Ahlrichs split-valence plus polarization basis sets (def2-SVP) on all atoms. Single point energies were then calculated with a TZVP basis set[33]. We used Gaussian09 Rev D.01[34] for these calculations. Collision cross-sections were calculated using an exact hard-spheres scattering model.[35]

RESULTS AND DISCUSSION

A solution of Eo-P (10 μM in H_2O) was injected in negative mode into the electrospray source.

Eo-P ions with charge states 5-, 4-, and 3- were observed. We focus on the quadruply charged species, further denoted $[Eo\text{-}P]^{4-}$. For tandem-IMS measurements, ions were accumulated and

then pulsed into the first drift tube (DT1) at a rate of ~10 Hz. At the end of DT1, a pulsed ion gate can be used to allow only ions with a specific mobility to pass. The selected ions were then trapped in a dual ion funnel assembly (DF B in Fig. 1) before injection in the second drift tube (DT2). Fig. 2d shows the full arrival time distribution (ATD) obtained (without selection) for $[Eo\text{-}P]^{4-}$. Three distinct peaks are observed, further denoted A, B and C, in increasing order of drift time. The corresponding experimental collision cross sections (CCS) are listed in Table 1.

Isomer-resolved collisional activation experiments were performed on each population of ions by applying a voltage drop between the two stages of the DF, *i.e.* after selection at the end of DT1, and before injection in DT2.[17] Comparison of the ATDs recorded after DT2 for different activation voltages (Fig. 2a to 2c) allows to probe interconversions between the different peaks.[36,37] After selection of peak A (Fig. 2a), isomerization toward peak B is observed even at low excitation voltage and is amplified at high excitation voltage. After selection of peak B, the reverse process is observed, although more limited (Fig. 2b). In this case, the fact that the ratio between peak A and peak B is essentially unaffected by the excitation voltage suggests that thermal isomerization between A and B occurs in DT2 and that the observed distribution reflects the equilibrium between the two populations of structures. When peak C is selected (Fig 2c), isomerization is only observed at high activation voltage leading to peaks B and, to a lesser extent, A. Altogether peak B corresponds to the most stable structures. Spontaneous isomerization between A and B is observed at room temperature, while more energy is required to convert C to A and B.

Optical action spectra for each family of structures were recorded by irradiating the mobility-selected ions in DF B. Peaks A and B were selected together, since they were found to spontaneously interconvert (*vide supra*). After laser excitation, the main relaxation channel for all species corresponds to electron detachment leading to the formation of a triply negatively charged radical ion.[38] The action-spectrum recorded for A and B (Fig. 3b) shows a band centered at 510 nm with a shoulder at 475 nm. The detachment yield is much lower for isomer C (Fig. 3c) leading to a broad band ranging from 460 to 540 nm. The origin of the differences between Fig. 3b and 3c can be understood with the examination of the action spectra recorded for $[Eo\text{-}P]^{5-}$ and $[Eo\text{-}P]^{3-}$ (Fig. 3a and d). In $[Eo\text{-}P]^{5-}$, the chromophore bears two negative charges while it bears a single charge in $[Eo\text{-}P]^{3-}$, as confirmed by spectra recorded for bare Eo^{-} and Eo^{2-} (Fig. 4).. The similarity between the action spectra recorded for $[Eo\text{-}P]^{5-}$ and peaks A and B of $[Eo\text{-}P]^{4-}$, and on the other hand for $[Eo\text{-}P]^{3-}$ and peak C of $[Eo\text{-}P]^{4-}$, suggests that the

different optical responses observed in Fig. 3c and 3d are due to the different charge state of the chromophore (doubly-charged in A and B, and singly-charged in C). The overall Fig. 3 suggests that for peaks A and B the Eo moiety is a dianion, while in C it is a monoanion.

Calculated structures for $[Eo\text{-}P]^{4-}$ were determined through force-field-based replica exchange molecular dynamics (REMD) calculations, followed by DFT optimizations. The most favorable deprotonation site on Eo-P is the hydroxyl group of Eo,[16] and is assumed to be deprotonated in all calculations. The 3 remaining charges were distributed between the 4 other possible sites, namely the carboxyl groups at the side chains of Glu (E) and Asp (D), on Eo and at the C terminus (C_t) (see scheme 1). The four corresponding isomers are named after the position of the carboxyl group which remains protonated. $Eo^{H}EDC_t$ stands for a singly-charged Eo, and deprotonated Asp, Glu, and C-terminus. The 3 other structures correspond to doubly deprotonated Eo with two additional charges on the peptide moiety (i.e. in $EoE^{H}DCt$ Asp residue remains protonated while Glu and C-terminus are deprotonated). Relative DFT energies and calculated CCS for the resulting four lowest-energy structures are given in Table 1, and shown in Fig. 5. The lowest-energy isomer corresponds to the $EoE^{H}DC_t$ configuration. All configurations with doubly-charged Eo lead to structures that are more compact than those with a singly-charged Eo ($Eo^{H}EDC_t$). In structures with Eo^{2-}, the protonated carboxyl group can form a hydrogen bond with one of the carboxylates (see Fig. 5), which favors proton transfer and subsequent interconversion between the different isomers with Eo^{2-}. When Eo is singly charged, the peptide moieties bear 3 charges and unfolds to minimize Coulomb repulsion between these 3 charges, which leads to high CCS. The resulting unfolded configurations do not display favorable structures for proton transfer, contrary to the ones for doubly-charged Eo (see Figure 5).

These theoretical results together with Fig. 2 and 3 (support that Eo is singly-charged in peak C, whereas it is doubly-charged in peaks A and B. We then assigned $Eo^{H}EDC_t$ to peak C and tentatively $EoE^{H}DC_t$ and $EoED^{H}C_t$ to the two other peaks. According to pKa values, a distribution of $Eo^{H}EDCt$, $EoE^{H}DCt$ and $EoED^{H}Ct$ is expected for 4- ions in solution. Despite the calculated high relative energy of $Eo^{H}EDCt$ in the gas phase, due to the high isomerization barrier (*vide supra*), it is possibly kinetically trapped from a solution structure. In this context, the small amount of conformer C that converts toward peaks A and B under collisional activation has undergone proton transfer from the Eo to the peptide moiety. A way to assess the occurrence of such a transfer is to measure the effect of light irradiation on the different peaks observed after collisional activation of ions in peak C. The ions that have experienced proton

transfer are expected to show optical properties comparable to those from ions in peaks A and B. After irradiation, they should thus be more efficiently depleted than the ions that have not undergone proton transfer. The ATD displayed at the top of Figure 6 was obtained after subjecting peak C ions to collisional activation followed by laser excitation at 520 nm. The ATD recorded without laser excitation, is reproduced on the same figure for comparison. The short-time shoulders, which are observed after collisional excitation and attributed to peaks A and B, are clearly found to decrease after laser excitation while the remaining intensity on peak C is very little affected. This is consistent with a switch in the optical response of the system following activated proton transfer (Scheme 2).

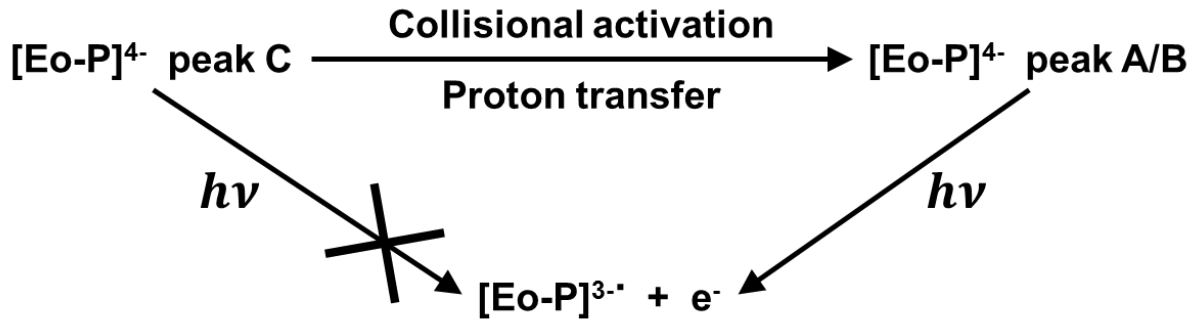

Scheme 2. Switch in photo-reactivity triggered by collision activated proton transfer.

In conclusion, we coupled mass-spectrometry, optical spectroscopy and ion mobility to explore the optical and structural properties of a peptide chain bound to a chromophore – a system with resemblance to blue to red-light receptor phototropins, phytochromes, and photo switchable proteins.[37,39,40] The use of both collision- and laser activation in a tandem-IMS scheme allowed us to probe how proton transfer between a peptide and its cofactor can dramatically modify optical properties of the system. We demonstrated the possibility of collisionally triggering this switch of optical properties. This opens new perspectives for gas phase structural biology[41,42] with the study of isolated analogous to photo-switchable native protein complexes.

Acknowledgements

The research leading to these results has received funding from the European Research Council under the European Union's Seventh Framework Programme (FP7/2007-2013 Grant agreement N°320659). AK acknowledges COST action BM1403.

References

(1) Takala, H.; Björling, A.; Berntsson, O.; Lehtivuori, H.; Niebling, S.; Hoernke, M.; Kosheleva, I.; Henning, R.; Menzel, A.; Ihalainen, J. A.; et al. Signal Amplification and Transduction in Phytochrome Photosensors. *Nature* **2014**, *509*, 245–248.

(2) Christie, J. M.; Blackwood, L.; Petersen, J.; Sullivan, S. Plant Flavoprotein Photoreceptors. *Plant Cell Physiol.* **2015**, *56*, 401–413.

(3) Harper, S. M.; Neil, L. C.; Gardner, K. H. Structural Basis of a Phototropin Light Switch. *Science* **2003**, *301*, 1541–1544.

(4) Schotte, F.; Cho, H. S.; Kaila, V. R. I.; Kamikubo, H.; Dashdorj, N.; Henry, E. R.; Graber, T. J.; Henning, R.; Wulff, M.; Hummer, G.; et al. Watching a Signaling Protein Function in Real Time via 100-Ps Time-Resolved Laue Crystallography. *Proc. Natl. Acad. Sci. U. S. A.* **2012**, *109*, 19256–19261.

(5) Pennacchietti, F.; Losi, A.; Xu, X.; Zhao, K.; Gärtner, W.; Viappiani, C.; Cella, F.; Diaspro, A.; Abbruzzetti, S. Photochromic Conversion in a Red/green Cyanobacteriochrome from Synechocystis PCC6803: Quantum Yields in Solution and Photoswitching Dynamics in Living E. Coli Cells. *Photochem. Photobiol. Sci.* **2015**, *14*, 229–237.

(6) Schäfer, L. V.; Groenhof, G.; Klingen, A. R.; Ullmann, G. M.; Boggio-Pasqua, M.; Robb, M. a.; Grubmüller, H. Photoswitching of the Fluorescent Protein asFP595: Mechanism, Proton Pathways, and Absorption Spectra. *Angew. Chem. Int. Ed.* **2007**, *46*, 530–536.

(7) Lindner, I.; Knipp, B.; Braslavsky, S. E.; Gärtner, W.; Schaffner, K. A Novel Chromophore Selectively Modifies the Spectral Properties of One of the Two Stable States of the Plant Photoreceptor Phytochrome. *Angew. Chem. Int. Ed.* **1998**, *37*, 1843–1846.

(8) Renner, C.; Alefelder, S.; Bae, J. H.; Budisa, N.; Huber, R.; Moroder, L. Fluoroprolines as Tools for Protein Design and Engineering. *Angew. Chem. Int. Ed.* **2001**, *40*, 923–925.

(9) Su, X.; Robbins, T. F.; Aprahamian, I. Switching through Coordination-Coupled Proton Transfer. *Angew. Chem. Int. Ed.* **2011**, *50*, 1841–1844.

(10) Schönberger, M.; Trauner, D. A Photochromic Agonist for μ-Opioid Receptors. *Angew. Chem. Int. Ed.* **2014**, *53*, 3264–3267.

(11) Tsai, Y.-H.; Essig, S.; James, J. R.; Lang, K.; Chin, J. W. Selective, Rapid and Optically Switchable Regulation of Protein Function in Live Mammalian Cells. *Nat. Chem.* **2015**, *7*, 554–561.

(12) Warnke, S.; Baldauf, C.; Bowers, M. T.; Pagel, K.; von Helden, G. Photodissociation of Conformer-Selected Ubiquitin Ions Reveals Site-Specific Cis/trans Isomerization of Proline Peptide Bonds. *J. Am. Chem. Soc.* **2014**, *136*, 10308–10314.

(13) Masson, A.; Kamrath, M. Z.; Perez, M. A. S.; Glover, M. S.; Rothlisberger, U.; Clemmer, D. E.; Rizzo, T. R. Infrared Spectroscopy of Mobility-Selected H+-Gly-Pro-Gly-Gly (GPGG). *J. Am. Soc. Mass Spectrom.* **2015**, *26*, 1444–1454.

(14) Coughlan, N. J. A.; Adamson, B. D.; Gamon, L.; Catani, K.; Bieske, E. J. Retinal Shows Its True Colours: Photoisomerization Action Spectra of Mobility-Selected Isomers of the Retinal Protonated Schiff Base. *Phys. Chem. Chem. Phys.* **2015**, *17*, 22623–22631.

(15) Markworth, P. B.; Adamson, B. D.; Coughlan, N. J. A.; Goerigk, L.; Bieske, E. J. Photoisomerization Action Spectroscopy: Flicking the Protonated Merocyanine–spiropyran Switch in the Gas Phase. *Phys. Chem. Chem. Phys.* **2015**, *17*, 25676–25688.

(16) Batistela, V. R.; Pellosi, D. S.; de Souza, F. D.; da Costa, W. F.; de Oliveira Santin, S. M.; de Souza, V. R.; Caetano, W.; de Oliveira, H. P. M.; Scarminio, I. S.; Hioka, N. pKa Determinations of Xanthene Derivates in Aqueous Solutions by Multivariate Analysis Applied to UV–Vis Spectrophotometric Data. *Spectrochim. Acta Part A Mol. Biomol. Spectrosc.* **2011**, *79*, 889–897.

(17) Simon, A.-L.; Chirot, F.; Choi, C. M.; Clavier, C.; Barbaire, M.; Maurelli, J.; Dagany, X.; MacAleese, L.; Antoine, R.; Dugourd, P. Tandem Ion Mobility Spectrometry Coupled to Laser Excitation: IMS Laser IMS. *Rev. Sci. Instrum.* **2015**, *86*, 094101–1 – 10.

(18) Revercomb, H. E.; Mason, E. A. Theory of Plasma Chromatography/Gaseous Electrophoresis- A Review. *Anal. Chem.* **1975**, *47*, 970–983.

(19) Daly, S.; Kulesza, A.; Poussigue, F.; Simon, A.-L.; Choi, C. M.; Knight, G.; Chirot, F.; MacAleese, L.; Antoine, R.; Dugourd, P. Conformational Changes in Amyloid-Beta (12–28) Alloforms Studied Using Action-FRET, IMS and Molecular Dynamics Simulations. *Chem. Sci.* **2015**, *6*, 5040–5047.

(20) Pearlman, D. A.; Case, D. A.; Caldwell, J. W.; Ross, W. S.; Cheatham, T. E.; DeBolt, S.; Ferguson, D.; Seibel, G.; Kollman, P. AMBER, a Package of Computer Programs for Applying Molecular Mechanics, Normal Mode Analysis, Molecular Dynamics and Free Energy Calculations to Simulate the Structural and Energetic Properties of Molecules. *Comp. Phys. Commun*. **1995**, *91*, 1–41.

(21) Wang, J.; Cieplak, P.; Kollman, P. a. How Well Does a Restrained Electrostatic Potential (RESP) Model Perform in Calculating Conformational Energies of Organic and Biological Molecules? *J. Comput. Chem.* **2000**, *21*, 1049–1074.

(22) Wang, J.; Wolf, R. M.; Caldwell, J. W.; Kollman, P. a.; Case, D. a. Development and Testing of a General Amber Force Field. *J. Comput. Chem.* **2004**, *25*, 1157–1174.

(23) Wang, J.; Wang, W.; Kollman, P. a; Case, D. a. Antechamber, An Accessory Software Package For Molecular Mechanical Calculations. *J. Comput. Chem.* **2005**, *25*, 1157–1174.

(24) Sugita, Y.; Okamoto, Y. Replica-Exchange Molecular Dynamics Method for Protein Folding. *Chem. Phys. Lett*. **1999**, *314*, 141–151.

(25) Van Der Spoel, D.; Lindahl, E.; Hess, B.; Groenhof, G.; Mark, A. E.; Berendsen, H. J. C. GROMACS: Fast, Flexible, and Free. *J. Comput. Chem.* **2005**, *26*, 1701–1718.

(26) Hess, B.; Kutzner, C.; van der Spoel, D.; Lindahl, E. GROMACS 4: Algorithms for Highly Efficient, Load-Balanced, and Scalable Molecular Simulation. *J. Chem. Theory Comput.* **2008**, *4* (3), 435–447.

(27) Kulesza, A.; Daly, S.; MacAleese, L.; Antoine, R.; Dugourd, P. Structural Exploration and Förster Theory Modeling for the Interpretation of Gas-Phase FRET Measurements: Chromophore-Grafted Amyloid-β Peptides. *J. Chem. Phys.* **2015**, *143*, 025101–1 – 8.

(28) Becke, A. Density Functional Thermochemistry III The Role of Exact Exchange. *J. Chem. Phys.* **1993**, *98*, 5648–5652.

(29) Perdew, J.; Burke, K.; Ernzerhof, M. Generalized Gradient Approximation Made Simple. *Phys. Rev. Lett.* **1996**, *77*, 3865–3868.

(30) Yanai, T.; Tew, D. P.; Handy, N. C. A New Hybrid Exchange-Correlation Functional Using the Coulomb-Attenuating Method (CAM-B3LYP). *Chem. Phys. Lett.* **2004**, *393*, 51–57.

(31) Grimme, S.; Ehrlich, S.; Goerigk, L. Effect of the Damping Function in Dispersion Corrected Density Functional Theory. *J. Comput. Chem.* **2011**, *32*, 1456–1465.

(32) Grimme, S.; Antony, J.; Ehrlich, S.; Krieg, H. A Consistent and Accurate Ab Initio Parametrization of Density Functional Dispersion Correction (DFT-D) for the 94 Elements H-Pu. *J. Chem. Phys.* **2010**, *132*, 154104–1 – 19.

(33) Weigend, F.; Ahlrichs, R. Balanced Basis Sets of Split Valence, Triple Zeta Valence and Quadruple Zeta Valence Quality for H to Rn: Design and Assessment of Accuracy. *Phys. Chem. Chem. Phys.* **2005**, *7*, 3297–3305.

(34) Gaussian 09 Revision D.01; Frisch, M. J.; Trucks, G. W.; Schlegel, H. B.; Scuseria, G. E.; Robb, M. A.; Cheeseman, J. R.; Scalmani, G.; Barone, V.; Mennucci, B.; et al. Gaussian 09 Revision D.01. Gaussian Inc. Wallingford CT 2009 p Gaussian Inc. Wallingford CT 2009.

(35) Shvartsburg, A. A.; Jarrold, M. F. An Exact Hard-Spheres Scattering Model for the Mobilities of Polyatomic Ions. *Chem. Phys. Lett.* **1996**, *261*, 86–91.

(36) Shi, H.; Atlasevich, N.; Merenbloom, S. I.; Clemmer, D. E. Solution Dependence of the Collisional Activation of Ubiquitin [M + 7H](7+) Ions. *J. Am. Soc. Mass Spectrom.* **2014**, *25*, 2000–2008.

(37) Dilger, J.; Musbat, L.; Sheves, M.; Bochenkova, A. V.; Clemmer, D. E.; Toker, Y. Direct Measurement of the Isomerization Barrier of the Isolated Retinal Chromophore. *Angew. Chem. Int. Ed.* **2015**, *54*, 4748–4752.

(38) Antoine, R.; Dugourd, P. Visible and Ultraviolet Spectroscopy of Gas Phase Protein Ions. *Phys. Chem. Chem. Phys.* **2011**, *13*, 16494–16509.

(39) Corchnoy, S. B.; Swartz, T. E.; Lewis, J. W.; Szundi, I.; Briggs, W. R.; Bogomolni, R. A. Intramolecular Proton Transfers and Structural Changes during the Photocycle of the LOV2 Domain of Phototropin 1. *J. Biol. Chem.* **2003**, *278*, 724–731.

(40) Toh, K. C.; Stojkovic, E. A.; van Stokkum, I. H. M.; Moffat, K.; Kennis, J. T. M. Proton-Transfer and Hydrogen-Bond Interactions Determine Fluorescence Quantum Yield and Photochemical Efficiency of Bacteriophytochrome. *Proc. Natl. Acad. Sci. U. S. A.* **2010**, *107*, 9170–9175.

(41) Rosati, S.; Rose, R. J.; Thompson, N. J.; van Duijn, E.; Damoc, E.; Denisov, E.; Makarov, A.; Heck, A. J. R. Exploring an Orbitrap Analyzer for the Characterization of Intact Antibodies by Native Mass Spectrometry. *Angew. Chem. Int. Ed.* **2012**, *51*, 12992–12996.

(42) Marcoux, J.; Robinson, C. V. Twenty Years of Gas Phase Structural Biology. *Structure* **2013**, *21*, 1541–1550.

Table 1. Calculated relative energies (ΔE) and CCS (calculated for the DFT-optimized structure and averaged over the T=292 K REMD ensemble) of $[Eo\text{-}P]^{4-}$ compared to the experimental values. Peak assignment (see Fig. 2d) is given in parenthesis. CCS values for doubly and singly charged Eosin Y are given for reference.

	ΔE [kJ/mol] DFT structure	CCS [Å^2] DFT structure	CCS [Å^2] REMD. av. value 292 K	CCS [Å^2] Exp. value (peak label)
$EoE^{H}DC_t$	0	347	359	382 ± 12 (B)
$EoED^{H}C_t$	+10	353	356	367± 12 (A)
$Eo^{H}EDC_t$	+55	387	396	399 ± 10 (C)
$EoEDC_t^{H}$	+30	374	391	--
Eo^{-}		142		139 ± 3
Eo^{2-}		143		148 ±3

Figure captions

Figure 1. General scheme of the apparatus. The inset details the dual-ion funnel (DF) assembly, denoted A, B, and C on the general scheme. The fourth funnel is the one implemented in the commercial Maxis Impact (Bruker). Laser and collision activations are performed in DF B.

Figure 2. Arrival time distributions (ATDs) recorded for $[Eo\text{-}P]^{4-}$ (d). 3 peaks are identified and labelled A, B and C. Results of selection and activation scans, where selection is applied to peak A (a), B (b), and C (c) (black line, excitation voltage 4V; red line excitation voltage 74V). 4V corresponds to the minimum value required for ion transfer and induces minimal excitation in this region. The curves at different activation energies have been normalized for comparison.

Figure 3. Action spectra recorded for $[Eo\text{-}P]^{5-}$ (a), $[Eo\text{-}P]^{4-}$ peaks A and B (b), $[Eo\text{-}P]^{4-}$ peak C (c). and $[Eo\text{-}P]^{3-}$ (d). (b) and (c) were obtained using the dual ion mobility set up. ATD for $[Eo\text{-}P]^{5-}$ and $[Eo\text{-}P]^{3-}$ display a single major peak. A linear ion trap was then used to record spectra in (a) and (d).[19]

Figure 4. Action spectra recorded for Eo^{-} (circles) and Eo^{2-} (squares).

Figure 5. Lowest-energy optimized structures for (a) $EoE^{H}DCt$, (b) $EoED^{H}Ct$, (c) $EoEDCt^{H}$ and (d) $Eo^{H}EDCt$ (CH and NH hydrogens, peptide bond oxygens as well as the Ala side chain omitted for clarity)

Figure 6. Selection scan ($[Eo\text{-}P]^{4-}$ Peak C, black line), activation scan (74 V, red line), activation scan (74 V) with addition of laser irradiation (λ = 520nm, green line). Laser irradiation is performed in DF after collisional activation. Blue dash lines were fitted on the red curve. They show the population of A, B and C after activation and before irradiation.

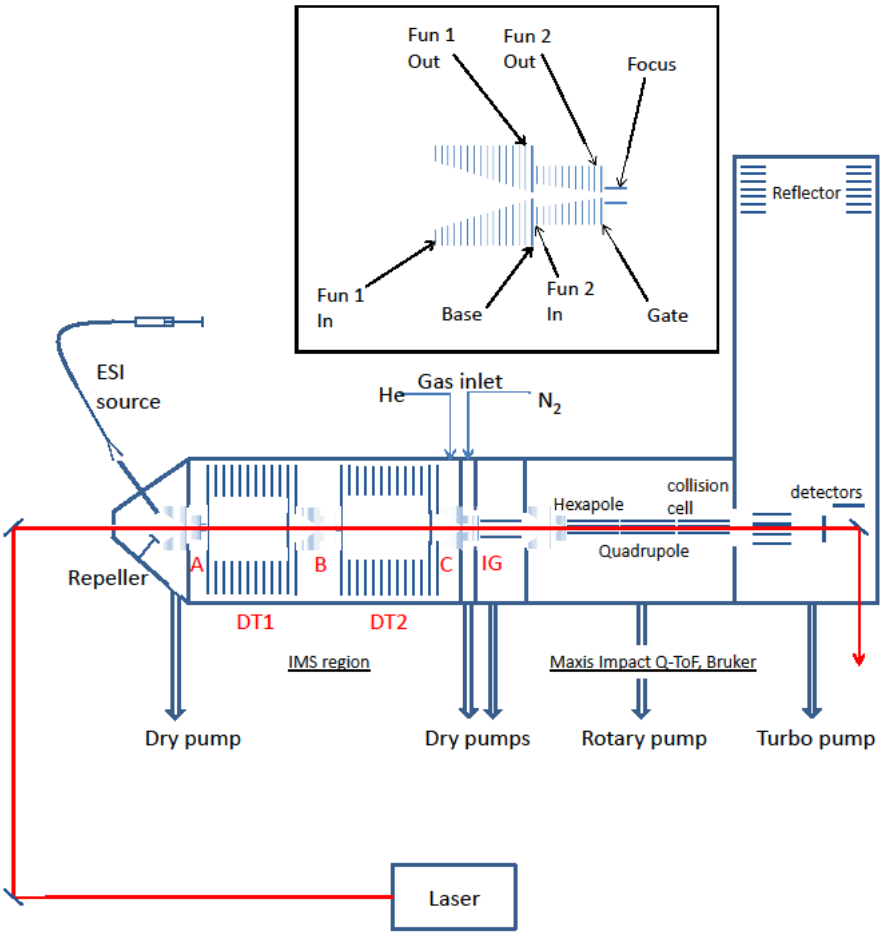
Fun 1
Out
Fun 2
Out
Focus
Reflector
Fun 1
In
Base
Fun 2
In
Gate
ESI
source
Gas inlet
He
N_2
Hexapole
collision
cell
detectors
Quadrupole
Repeller
A
B
C
IG
DT1
DT2
IMS region
Maxis Impact Q-ToF, Bruker
Dry pump
Dry pumps
Rotary pump
Turbo pump
Laser

Figure 1

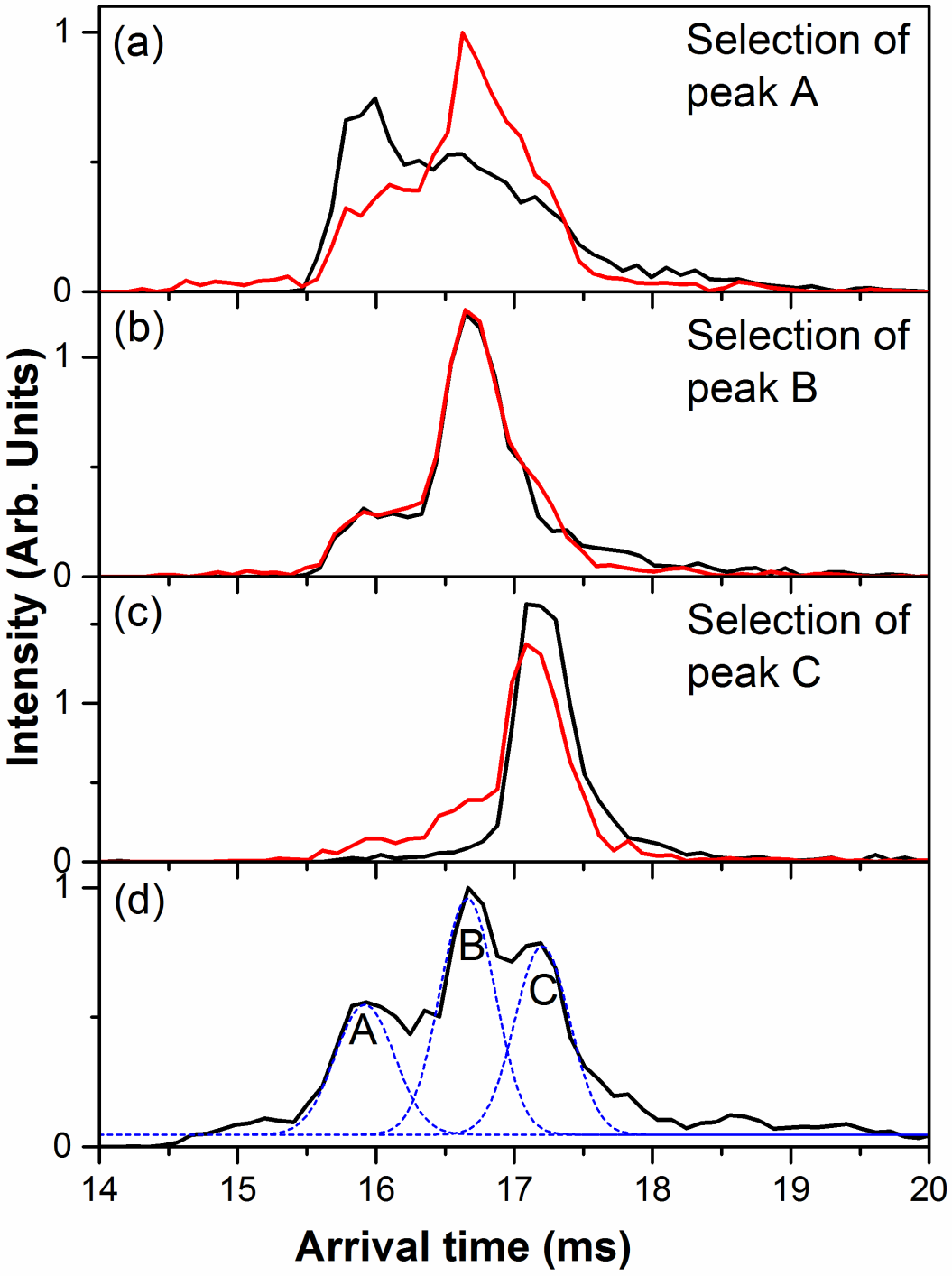
(a)
Selection of peak A
(b)
Selection of peak B
(c)
Selection of peak C
(d)
A
B
C
Intensity (Arb. Units)
Arrival time (ms)
0
1
14
15
16
17
18
19
20

Figure 2

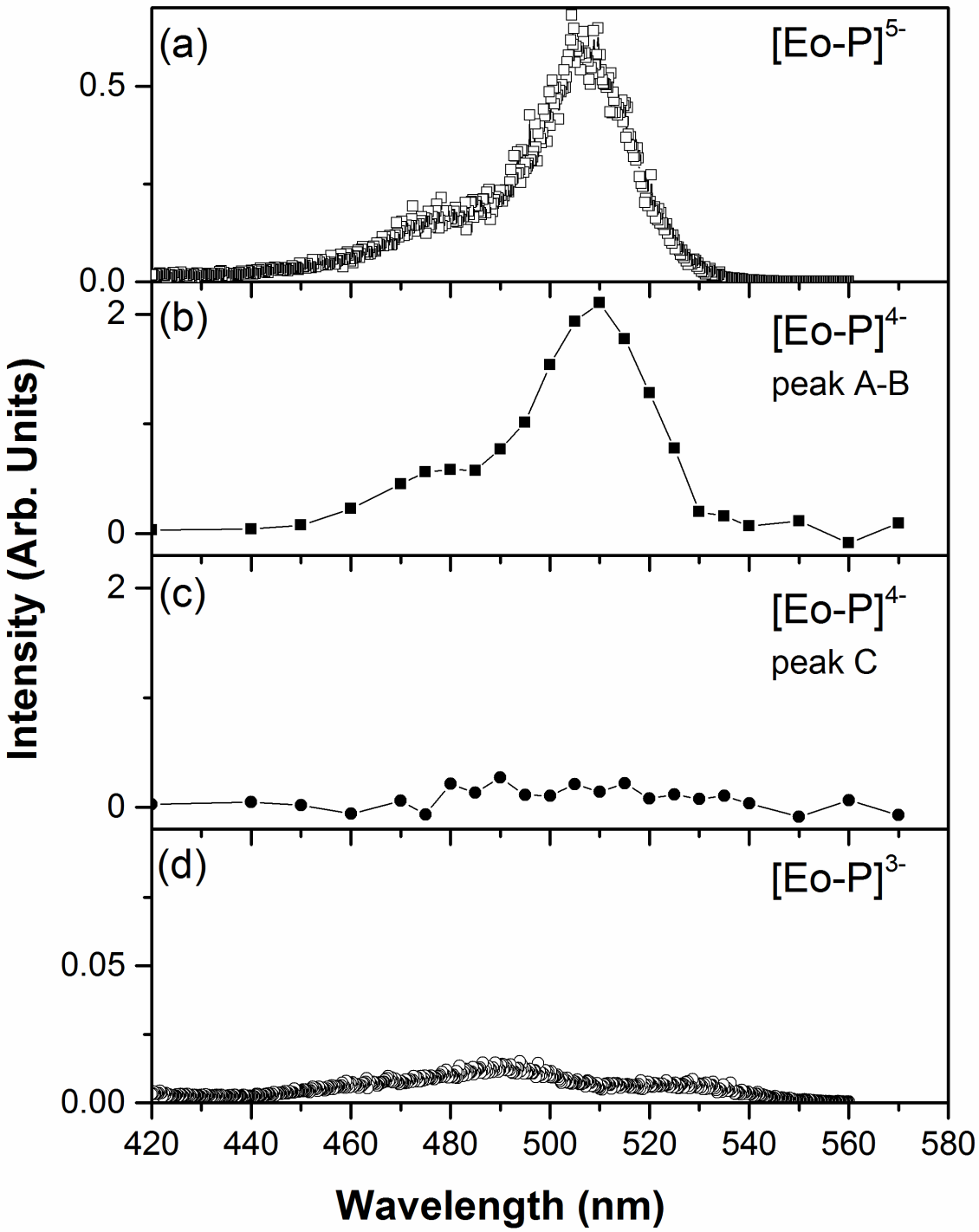
(a)
[Eo-P]5-
0.5
0.0
(b)
[Eo-P]4-
peak A-B
2
0
(c)
[Eo-P]4-
peak C
2
0
(d)
[Eo-P]3-
0.05
0.00
Intensity (Arb. Units)
420
440
460
480
500
520
540
560
580
Wavelength (nm)

Figure 3

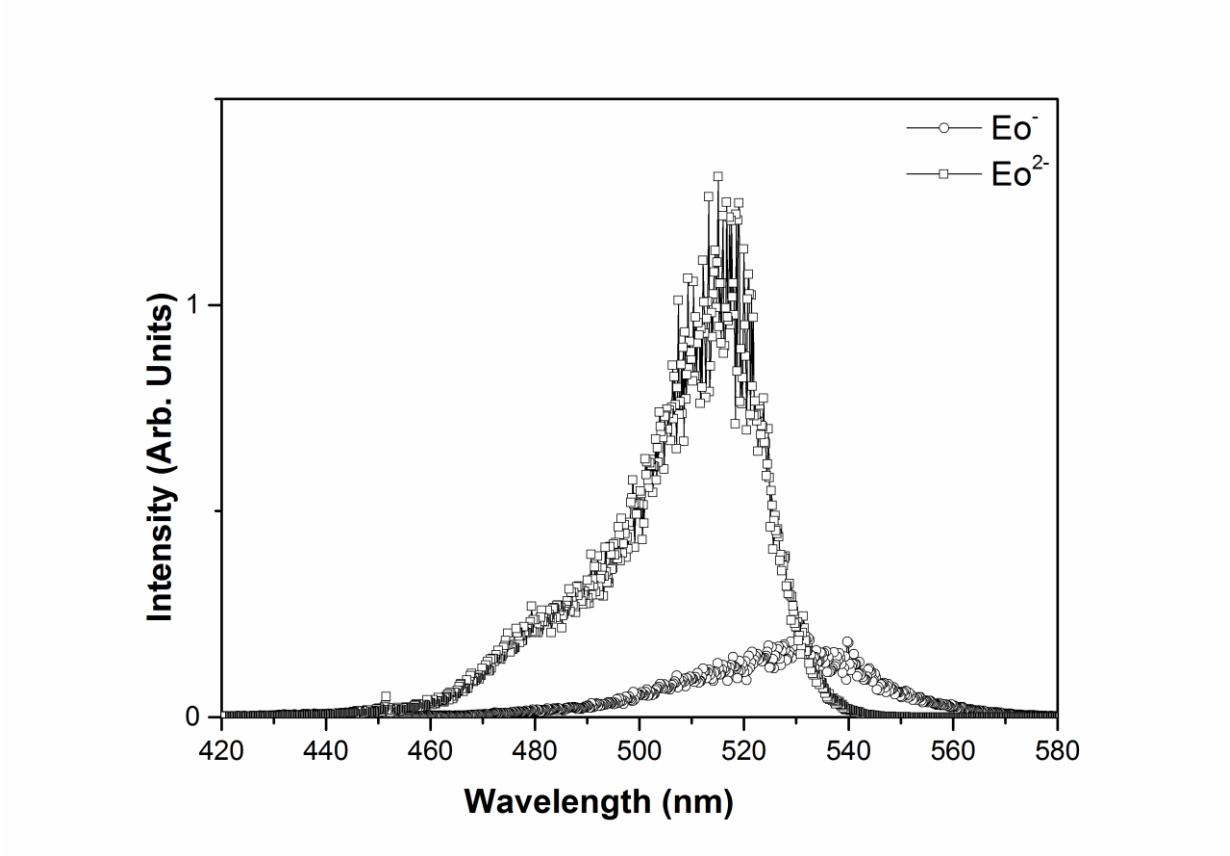
Eo-
Eo2-
Intensity (Arb. Units)
0
1
420
440
460
480
500
520
540
560
580
Wavelength (nm)

Figure 4

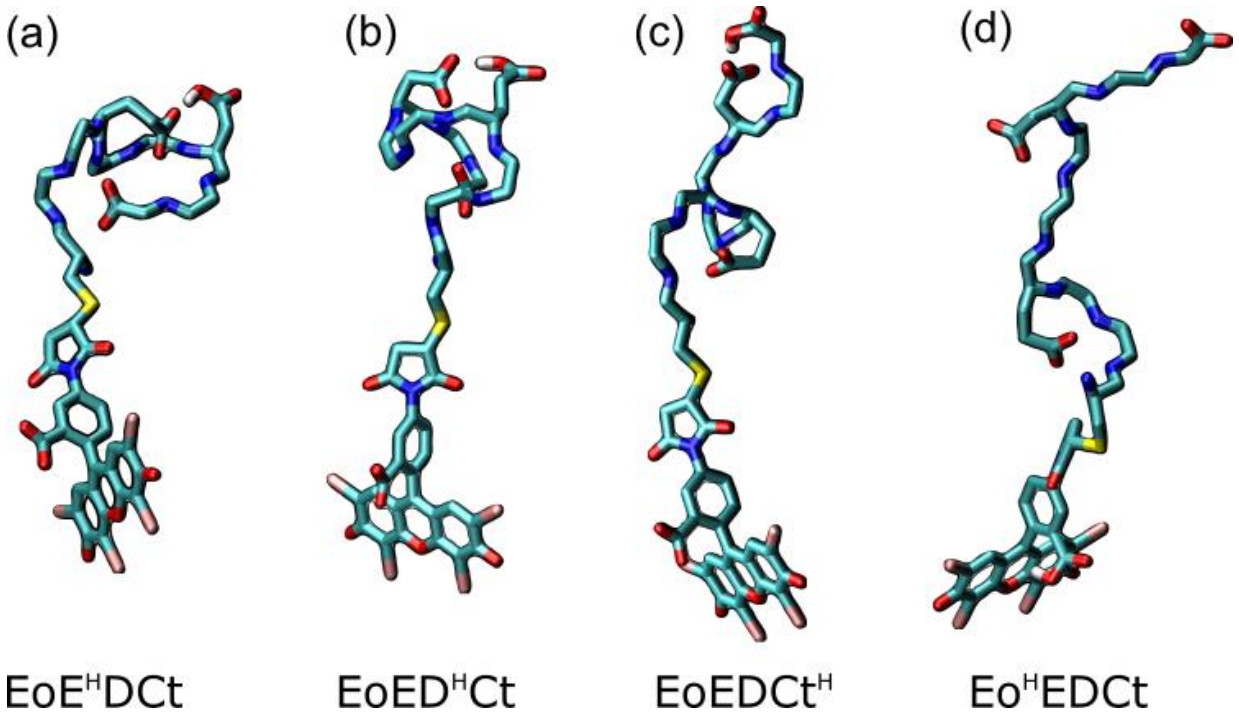

Figure 5

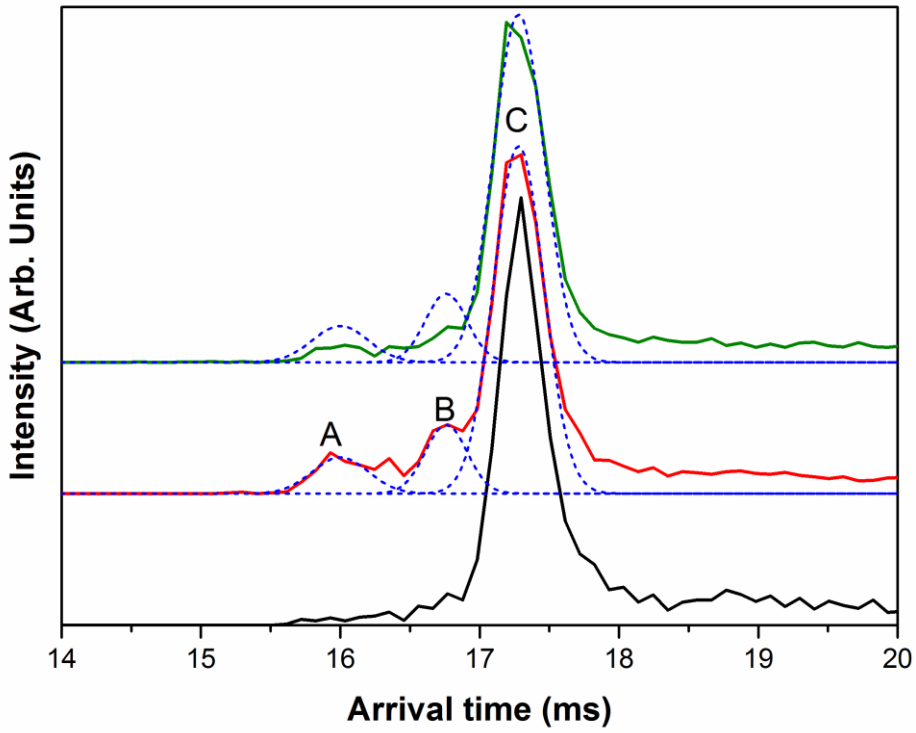

Figure 6